The *Arabidopsis* SAFEGUARD1 suppresses singlet oxygen-induced stress responses by protecting grana margins

Liangsheng Wang[a,b,1], Dario Leister[a], Li Guan[c], Yi Zheng[b], Katja Schneider[d], Martin Lehmann[a], Klaus Apel[b], and Tatjana Kleine[a]

[a]Plant Molecular Biology (Botany), Faculty of Biology, Ludwig-Maximilians-Universität München, 82152, Planegg-Martinsried, Germany; [b]Boyce Thompson Institute, Ithaca, NY 14853-1801; [c]Department Biology I, Botanik, Ludwig-Maximilians-Universität München, 82152, Planegg-Martinsried, Germany; and [d]Department Biology I, Plant Development, Ludwig-Maximilians-Universität München, 82152, Planegg-Martinsried, Germany

Edited by Christine Foyer, University of Leeds, Leeds, United Kingdom, and accepted by Editorial Board Member Julian I. Schroeder February 14, 2020 (received for review October 24, 2019)

Singlet oxygen ($^1O_2$), the major reactive oxygen species (ROS) produced in chloroplasts, has been demonstrated recently to be a highly versatile signal that induces various stress responses. In the *fluorescent* (*flu*) mutant, its release causes seedling lethality and inhibits mature plant growth. However, these drastic phenotypes are suppressed when EXECUTER1 (EX1) is absent in the *flu ex1* double mutant. We identified SAFEGUARD1 (SAFE1) in a screen of ethyl methanesulfonate (EMS) mutagenized *flu ex1* plants for suppressor mutants with a *flu*-like phenotype. In *flu ex1 safe1*, all $^1O_2$-induced responses, including transcriptional rewiring of nuclear gene expression, return to levels, such as, or even higher than, those in *flu*. Without SAFE1, grana margins (GMs) of chloroplast thylakoids (Thys) are specifically damaged upon $^1O_2$ generation and associate with plastoglobules (PGs). SAFE1 is localized in the chloroplast stroma, and release of $^1O_2$ induces SAFE1 degradation via chloroplast-originated vesicles. Our paper demonstrates that *flu*-produced $^1O_2$ triggers an EX1-independent signaling pathway and proves that SAFE1 suppresses this signaling pathway by protecting GMs.

singlet oxygen | chloroplast | stress | retrograde signaling | SAFEGUARD1

Plants have to cope with various reactive oxygen species (ROS) which are continuously produced in cell organelles, especially in chloroplasts (1, 2). ROS can damage lipids, DNA, proteins, and other biological components. Correspondingly, plants have evolved a variety of mechanisms to detoxify ROS or protect against its effects, including low-molecular-weight antioxidants (e.g., carotenoids, flavonoids, plastoquinones, tocopherols, ascorbate, and glutathione) and scavenging enzymes (e.g., superoxide dismutase, ascorbate peroxidase, glutathione peroxidase, and catalase) (1, 3). However, under stress conditions, such as drought, high light (L), or pathogen attack, this balanced network of ROS production and degradation is frequently disturbed, favoring the production of ROS. Recent studies have demonstrated that ROS are also beneficial for plants since they are crucial for the regulation of several important biological processes, particularly, in cell differentiation and stress tolerance (4–7).

The ROS singlet oxygen ($^1O_2$), which is responsible for most photo-oxidative damage in chloroplasts (8) and has long been recognized as a cytotoxin that inhibits photosynthesis and compromises cell function, also acts as a highly versatile signal that induces various stress responses (9–12). $^1O_2$ was first shown to regulate the expression of the glutathione peroxidase homologous (*Gpxh*) gene in *Chlamydomonas reinhardtii* (13). Two years later, a broader significance for $^1O_2$ as a signaling molecule was described in the study of the conditional *fluorescent* (*flu*) mutant of *Arabidopsis thaliana* (9). *FLU* encodes a negative regulator of tetrapyrrole biosynthesis, and the *flu* mutant lacking this regulator is unable to constrain accumulation of protochlorophyllide ([Pchlide], an intermediate of chlorophyll biosynthesis) in the dark (D) (14, 15). When D-adapted *flu* plants are transferred to L, the photosensitizing Pchlide molecules can transfer L energy to ground-state (triplet) molecular oxygen ($^3O_2$), leading to the generation of $^1O_2$. A burst of $^1O_2$ in the *flu* mutant upon exposure to L induces bleaching of young seedlings and growth inhibition in mature plants. However, all these phenotypic changes can be suppressed by inactivation of the *EX1* gene. Upon a D–L shift, *flu ex1* mutants generate similar amounts of $^1O_2$ to parental *flu* plants but show no obvious $^1O_2$-induced stress responses, indicating a signaling role for $^1O_2$ in the latter (10, 16). In the *flu* mutant, $^1O_2$ generated in thylakoids (Thys) oxidizes the Trp643 residue of EX1. Subsequent FtsH2-dependent cleavage of the oxidized EX1 protein is necessary for induction of this signaling pathway (17–19). A quite recent study using the *Arabidopsis lesion simulating disease1* (*lsd1*) mutant points out that uncoupled expression of nuclear and plastid photosynthesis-associated genes disrupts the stoichiometry of photosynthetic proteins,

Significance

Singlet oxygen ($^1O_2$) generated in the *Arabidopsis fluorescent* (*flu*) mutant triggers cell death in young seedlings and inhibits growth of mature plants through the EXECUTER1 (EX1)-dependent retrograde signaling pathway. Here, we show another $^1O_2$-induced chloroplast-to-nucleus retrograde signaling pathway, the $^1O_2$-SAFEGUARD1 (SAFE1) pathway that is independent of EX1. SAFE1 is localized in the chloroplast stroma, and release of $^1O_2$ induces SAFE1 degradation via chloroplast-originated vesicles. Without SAFE1, grana margins (GMs) of chloroplast thylakoids are specifically damaged upon $^1O_2$ generation and associate with plastoglobules. We suggest that the *Arabidopsis* SAFE1 suppresses $^1O_2$-induced stress responses by protecting GMs. Our paper, therefore, uncovers an additional $^1O_2$-induced pathway and a unique mechanism by which higher plants deal with oxidative stress.

Author contributions: L.W. and K.A. designed research; L.W., L.G., and K.S. performed research; L.W., D.L., K.A., and T.K. contributed new reagents/analytic tools; L.W., Y.Z., M.L., and T.K. analyzed data; and L.W., D.L., and T.K. wrote the paper.

The authors declare no competing interest.

This article is a PNAS Direct Submission. C.F. is a guest editor invited by the Editorial Board.

Data deposition: Sequencing data have been deposited in the National Center for Biotechnology Information (NCBI) Gene Expression Omnibus (GEO) database, https://www.ncbi.nlm.nih.gov/geo (accession no. GSE131610).

[1]To whom correspondence may be addressed. Email: liangsheng.wang@lmu.de.

This article contains supporting information online at https://www.pnas.org/lookup/suppl/doi:10.1073/pnas.1918640117/-/DCSupplemental.

First published March 11, 2020.

resulting in the generation of $^1O_2$ in chloroplasts and a weak cell-death phenotype. The cell-death phenotype of the *lsd1* mutant relies on the presence of the EX1 protein (20). Meanwhile, more conditional mutants that selectively induce generation of $^1O_2$ were isolated. The *Arabidopsis ferrochelatase2* (*fc2*) mutant is defective in converting of protoporphyrin IX (ProtoIX) to heme, and the elevated level of ProtoIX acts as a photosensitizer and generates $^1O_2$ that damages chloroplasts (11, 21). The damaged chloroplasts are then ubiquitinated on the outer envelope via PUB4 ubiquitin ligase and degraded (11, 22). Another experimental system is the *Arabidopsis* chlorophyll *b*-less *chlorina* (*ch1*) mutant that is devoid of PSII antenna complexes (23). The *ch1* mutant is hypersensitive to high L due to a selective increase in $^1O_2$ in the reaction center (RC) of PSII in the grana core (GC) (appressed regions of the grana) (23). The cell-death response of the *ch1* mutant to high L can be partially rescued by inactivation of the *oxidative signal inducible* (*OXI1*) gene (12). Not only interruptions of chlorophyll biosynthesis, but also disturbances of chlorophyll catabolism favor production of $^1O_2$. The *Arabidopsis ACD2* encodes a chlorophyll catabolite reductase (RCCR) that can breakdown red chlorophyll catabolite (RCC), an intermediate in the chlorophyll breakdown process, and the mutant lacking RCCR accumulates RCC and releases $^1O_2$, inducing programmed cell death in mature leaves (24, 25).

The *flu ex1* double mutant is an ideal tool for exploring $^1O_2$-induced signaling in plants since it can specifically generate $^1O_2$ but shows no obvious phenotypic changes. In addition, the amount of $^1O_2$ generated in *flu ex1* is positively correlated with the duration of D treatment (26). For up to 8-h D treatment, $^1O_2$ generated in *flu ex1* after transfer to L is too low to damage the cell directly, and the signaling effect of $^1O_2$ is suppressed by the EX1 mutation, causing no obvious phenotypic changes (27). Here, we employed *flu ex1* as a starting material to explore $^1O_2$-mediated signaling in *Arabidopsis*. We identified a retrograde signaling pathway that negatively regulates $^1O_2$-mediated stress responses and proved the GMs were the first targets of $^1O_2$. Besides, our work also demonstrated that this $^1O_2$-induced retrograde signaling pathway was suppressed by the stroma protein SAFEGUARD1 (SAFE1)-mediated protection of GMs.

Results

Identification of *flu ex1 safe1* Mutants and the *SAFE1* Gene. To further explore and identify components of $^1O_2$-induced signaling, we mutagenized the *flu ex1* mutant with EMS and screened the M2 generation for mutants that restored the $^1O_2$-induced cell-death phenotype. A group of four recessive mutants that behaved like *flu* when kept under nonpermissive D–L growth conditions was isolated (Fig. 1 and *SI Appendix*, Fig. S1). Allelism tests revealed that these represented alleles of the same locus, which was named *SAFE1* because its normal product protects the *flu ex1* mutant from $^1O_2$-induced damage. A combination of next-generation sequencing and map-based cloning revealed that the four allelic *flu ex1 safe1* mutants harbored mutations in the gene *At5g14260* (*SI Appendix*, Fig. S2 *A–E*). The *SAFE1* mutation in *At5g14260* was verified by complementation of the *flu ex1 safe1* phenotype with SAFE1-YFP, SAFE1-Myc, and SAFE1-GUS fusion proteins (*SI Appendix*, Fig. S2*F*).

The *flu ex1 safe1* Mutants Are Hypersensitive to *flu*-Generated $^1O_2$. Like the *flu* mutant, mature *flu ex1 safe1* plants ceased to grow when exposed to a nonpermissive L–D regime (Fig. 1 *A* and *B* and *SI Appendix*, Fig. S1), and young *flu ex1 safe1* seedlings displayed a cell-death phenotype (Fig. 1 *C–E*). The incidence of cell death revealed by trypan blue staining was correlated with the level of Pchlide accumulation in leaves (Fig. 1 *C–G*). In *flu ex1 safe1* seedlings, Pchlide accumulation was proportional to the duration of D treatment (Fig. 1*G*), indicating that more $^1O_2$ was generated after reillumination if plants had been incubated in the D for longer times. The increased $^1O_2$ content caused enhanced cell death, in association with pronounced decreases in transient chlorophyll fluorescence and maximum photochemical efficiency (F_v/F_m) of PSII (Fig. 1 *C–F*). In mature *flu ex1 safe1* plants, Pchlide mainly accumulated in emerging leaves when incubated in the D and caused severe cell death in these leaves after reillumination (*SI Appendix*, Fig. S3). In contrast, when grown under continuous L, both *flu* and *flu ex1 safe1* behaved exactly like wild-type (WT) plants (Fig. 1 *B–F* and *SI Appendix*, Figs. S1 and S4).

During D treatment, the *flu ex1 safe1* mutants produced the same amount of Pchlide as *flu* plants (Fig. 1 *H* and *I*) and generated similar amounts of $^1O_2$ after reillumination (Fig. 1*J*). However, the *flu ex1 safe1* mutants showed a more severe cell-death phenotype in both seedlings and young leaves of mature plants after release of $^1O_2$ than did the *flu* mutant (Fig. 1 *C–F* and *SI Appendix*, Fig. S3). However, the SAFE1 protein apparently does not play a significant role in plants under high-L stress since the *safe1* single mutant, *flu safe1* double mutant, and *flu ex1 safe1* triple mutant were phenotypically indistinguishable from the WT, and photosynthetic performance was not affected in these plants (*SI Appendix*, Fig. S5).

SAFE1 Suppresses $^1O_2$-Induced Transcriptional Changes. A burst of $^1O_2$ induces widespread changes in gene expression in the *flu* mutant (9), and this $^1O_2$-induced transcriptional response is largely suppressed in *flu ex1* (28). However, in *flu ex1 safe1*, the $^1O_2$-induced alterations at the transcriptional level were comparable to those seen in the *flu* mutant (Fig. 2). This was revealed by comparison of our RNA-sequencing (RNA-seq) data for 6-d-old *flu ex1* and *flu ex1 safe1* seedlings which were incubated in the D for 4 h and reilluminated for 30 or 60 min, respectively, with previously generated RNA-seq data for the *flu* mutant (18), grown under the same conditions (Fig. 2*A* and Datasets S1–S5). About half of the greater than twofold-induced genes in the *flu* mutant after release of $^1O_2$ were also induced more than twofold in *flu ex1 safe1* by $^1O_2$ (Fig. 2*B*). A group of 566 genes was greater than twofold induced in *flu ex1 safe1* but not in *flu ex1* after 30 and 60 min of reillumination, and we designated this gene set as "*induced by removal of SAFE1*" or "*reSAFE1*" (Fig. 2*C* and Dataset S6). Gene ontology analysis showed that stress-, immune-, and defense-related genes were highly enriched in *reSAFE1* (*SI Appendix*, Fig. S6*A*). Similarly, *reSAFE1* highly overlaps not only with the sets induced by $^1O_2$ in the *flu* (18) and *ch1* mutants (23), but also with genes induced by pathogen attack in WT plants (Fig. 2*D* and *SI Appendix*, Fig. S6*B*). Moreover, *reSAFE1* overlaps moderately with genes that are differentially expressed after β-CC treatment (29) or a low GSH state (30) and only to a small extent with genes differentially expressed after exposure to H_2O_2 or high L (31) (Fig. 2*D*). The RNA-seq data were confirmed by measuring the relative change in mRNA expression of representative genes (Fig. 2*E*). In *ex1*, *safe1*, and *ex1 safe1*, the expression of the four genes was not affected after a D–L shift because no $^1O_2$ was generated under these conditions, but they were all highly induced by $^1O_2$ in *flu*, *flu safe1*, and *flu ex1 safe1* with the highest expression in *flu safe1* (Fig. 2*E*).

GMs Are Specifically Damaged by $^1O_2$ When SAFE1 Is Not Present. Previous studies showed that $^1O_2$ was generated at chloroplast Thys in the *flu ex1* mutant (17), but the consequence of this $^1O_2$ generation on the structure of chloroplasts is still unclear. Thus, we analyzed the ultrastructure of chloroplasts from *flu*, *flu ex1*, and *flu ex1 safe1-5* before and after $^1O_2$ generation. Release of $^1O_2$ in *flu* seedlings resulted in chloroplasts with shrunken shape and low-staining vesicles and induced degradation of chloroplasts. Whereas in *flu ex1*, these changes were all suppressed (Fig. 3*A*). The numbers and sizes of plastoglobules (PGs) in both *flu* and *flu ex1* seedlings were not significantly affected by $^1O_2$

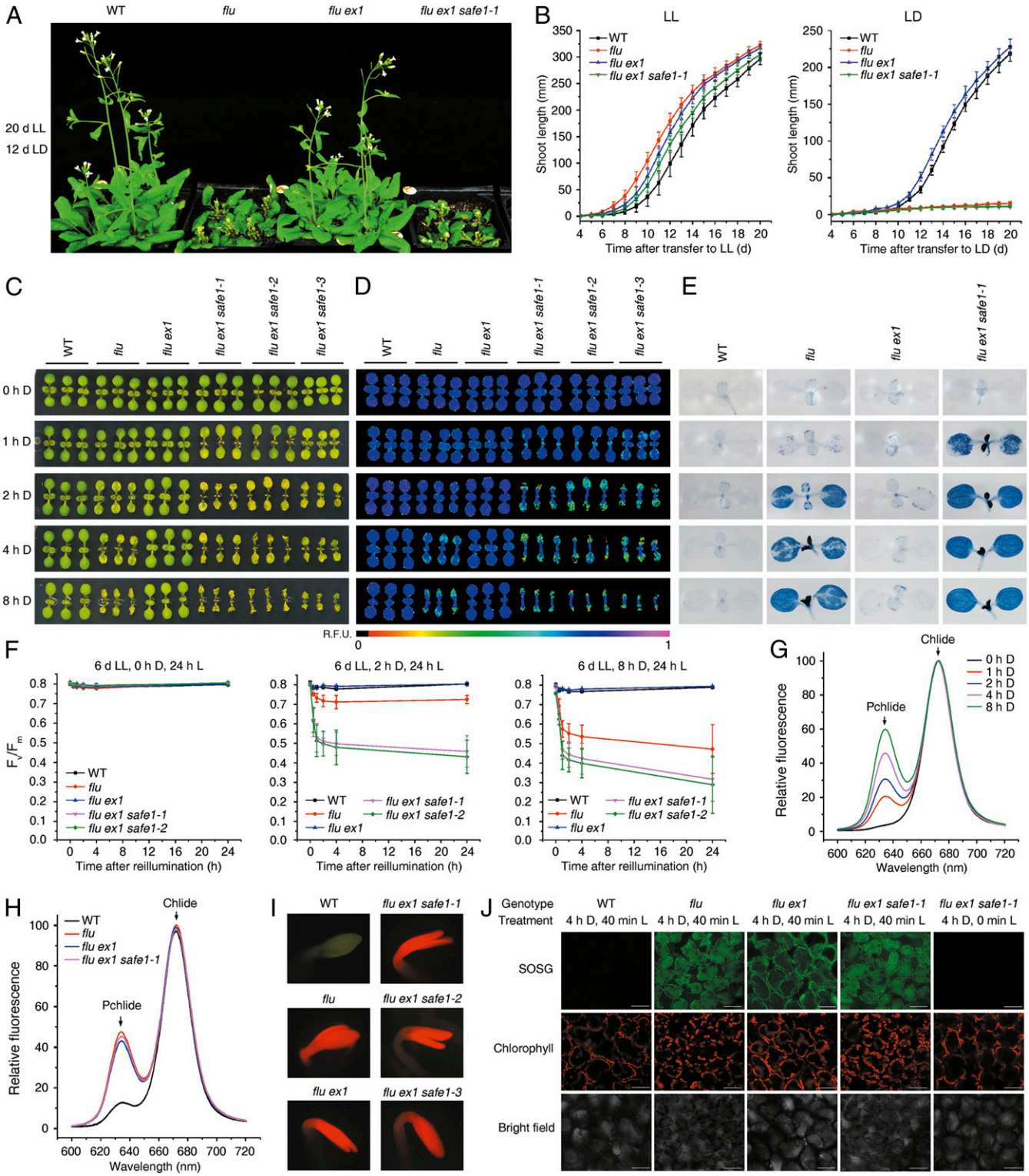

Fig. 1. SAFE1 suppresses stress responses triggered by $^1O_2$ signaling. (*A*) Mutation of *SAFE1* in *flu ex1* restores $^1O_2$-induced growth inhibition. Plants were grown under continuous light (LL), then exposed to a L–D regime (LD) as indicated. (*B*) Growth rates of the genotypes in *A* under LL (*Left*) or LL followed by LD (*Right*). (*C*–*E*) Impact of enhanced $^1O_2$ generation during extended D periods on cotyledon bleaching (*C*), chlorophyll autofluorescence (*D*), cell death (*E*), and maximum PSII efficiency (F_v/F_m) (*F*). Mean values ± SDs ($n > 30$) are provided. (*G*) Levels of Pchlide and chlorophyllide (Chlide) in *flu ex1 safe1-1* following various periods of D incubation, determined on the basis of their fluorescence emission at 634 and 673 nm, respectively. (*H*) Pchlide and Chlide accumulation in WT, *flu*, *flu ex1*, and *flu ex1 safe1-1* after 4 h of D incubation. (*I*) Direct visualization of Pchlide accumulation in 4-d-old etiolated seedlings, based on its characteristic red fluorescence under blue L. (*J*) Quantification of $^1O_2$ in seedlings based on the $^1O_2$ sensor green (SOSG) assay. Seedlings were first grown under LL, D incubated for 4 h, and then reexposed to L.

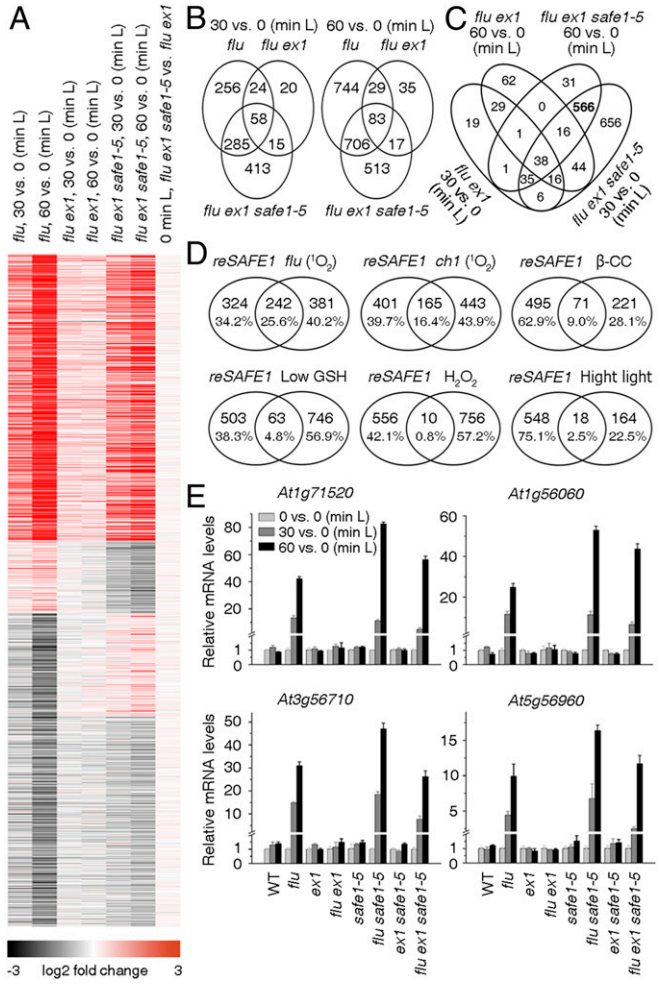

Fig. 2. $^1O_2$-induced changes in gene expression in *flu ex1 safe1* are recovered to those seen in the *flu* mutant. (*A*) $^1O_2$-induced changes in gene expression in *flu*, *flu ex1*, and *flu ex1 safe1–5* plants. Before release of $^1O_2$ (0-min L), no significant differences in gene expression were detected between *flu ex1 safe1–5* and *flu ex1* (last panel). Release of $^1O_2$ was achieved by exposing D-incubated seedlings (4 h) to L for 30 or 60 min. (*B*) Venn diagrams showing the numbers of genes that were up-regulated greater than or equal to twofold in *flu*, *flu ex1*, and *flu ex1 safe1–5* reexposed to L for 30 min or 60 min, respectively. (*C*) A set of 566 genes (indicated in bold and designated *reSAFE1*) is specifically regulated in *flu ex1 safe1–5* (compared to *flu ex1*) after release of $^1O_2$. (*D*) The *reSAFE1* set displays large overlaps with genes regulated by $^1O_2$ in *flu* (18) and *ch1* (23) lines, moderate overlaps with genes induced by β-cyclocitral (β-CC) (29) or low glutathione (GSH) (30), and little overlap with genes induced by H_2O_2 (31) or high-L stress (31). (*E*) Quantitative RT-PCR expression analysis of selected genes. Transcript levels were normalized with respect to *Actin2*. Mean values ± SDs ($n = 3$) are provided.

(Fig. 3*A*). However, in *flu ex1 safe1* seedlings, both numbers and sizes of PGs were dramatically increased after release of $^1O_2$ (Fig. 3*A*). Enlargement of electron micrographs revealed that PGs were randomly distributed on the Thys of *flu* and *flu ex1* seedlings (Fig. 3*B*). But in *flu ex1 safe1* seedlings after release of $^1O_2$, several PGs clustered and fused with each other and, together with Thy stacks, they formed dumbbell-shaped conglomerates on GMs (Fig. 3*B* and *SI Appendix*, Fig. S7). We suspected that GMs might be specifically damaged upon release of $^1O_2$ when SAFE1 was not present in *flu ex1*. To test this, levels of representative proteins known to be enriched in the GC, GMs, or stroma lamellae (SL) (17) were quantified after release of $^1O_2$. Levels of protochlorophyllide oxidoreductase (POR), curvature Thy1 (CURT1), Mg^{2+}-chelatase subunit I (CHLI), and Mg^{2+}-protoporphyrin IX methyl transferase (CHLM), which are representative proteins enriched in the GM (Fig. 3*C*), decreased drastically after release of $^1O_2$ (Fig. 3*D*). In contrast, levels of PSII RC protein A (D1) and PSII RC protein D (D2)—normally enriched in the GC (Fig. 3*C*)—were apparently not significantly affected by $^1O_2$ (Fig. 3*D*).

These findings indicate that, in *flu ex1 safe1*, the GM is quickly and severely damaged upon release of $^1O_2$, resulting in accumulation of PGs on damaged GMs. In *flu ex1*, presumably due to the protective effect of SAFE1, the GMs were not obviously affected by $^1O_2$, PGs did not accumulate, and chloroplasts remained intact and functional, suggesting that the GMs were the first target of $^1O_2$, and SAFE1 protects GMs from $^1O_2$-induced damage.

$^1O_2$ Induces Degradation of the Stroma-Localized SAFE1 Protein. Since the localization of a protein is tightly linked with its function, we tested the localization of SAFE1 using stable *pSAFE1::SAFE1-GUS*, *pSAFE1::SAFE1-YFP*, and *pSAFE1::SAFE1-Myc* transgenic plants (all in the Columbia [Col-0] background). The results showed that the SAFE1-GUS fusion protein was expressed in all of the organs except the petal (Fig. 4*A*). Subcellular analysis revealed that SAFE1-YFP was localized in chloroplasts (Fig. 4*C*). Subsequently, chloroplasts from *pSAFE1::SAFE1-YFP* and *pSAFE1::SAFE1-Myc* transgenic plants were further fractionated into the membrane and stroma which were then analyzed by immunoblotting. The result showed that SAFE1 was present in the chloroplast stroma (Fig. 4*B*). In the WT (*pSAFE1::SAFE1-YFP* Col-0), SAFE1 was evenly distributed in the chloroplasts as no $^1O_2$ was generated. A sudden release of $^1O_2$ in the *flu* mutant (*pSAFE1::SAFE1-YFP flu*) led to chloroplast rupture. However, in the *flu ex1* double mutant (*pSAFE1::SAFE1-YFP flu ex1*), its release did not alter the integrity of the chloroplast but induced formation of chloroplast-originated SAFE1-containing vesicles (Fig. 4 *C* and *D*). In addition to SAFE1, these vesicles also contained Rubisco (*SI Appendix*, Fig. S8) and Thy membranes—judged from the red chlorophyll autofluorescence (Fig. 4 *C* and *D*). The formation of SAFE1-containing vesicles occurred within 1 h, increased slightly until 4 h after $^1O_2$ generation, and declined significantly when seedlings were exposed to L for 8 h and reached the basal level after 16 h in the L (Fig. 4*E*). However, only a small fraction of SAFE1 was degraded in *flu ex1* after the release of $^1O_2$ because the majority of the SAFE1-YFP protein was still retained in chloroplasts (Fig. 4 *C* and *D*), and the overall SAFE1 protein content in plants was not dramatically affected by $^1O_2$ as evidenced by immunoblotting of SAFE1-YFP (Fig. 4*F*).

SAFE1 Is Not Involved in Methylation of Rubisco. SAFE1 is annotated as a Rubisco methyltransferase family protein (https://www.arabidopsis.org/). Therefore, the methylation status of Rubisco complexes from *flu ex1* and *flu ex1 safe1–5* were determined by mass spectrometry. Three methylation sites in two peptides were found in the RbcL subunit, but their methylation status was essentially unaffected (*SI Appendix*, Fig. S9). This result is compatible with previous studies in which the purified SAFE1 protein (named AtPPKMT1) showed no significant binding to Rubisco and was unable to methylate Rubisco or chloroplastic aldolases in vitro (32, 33). These findings suggest that SAFE1 is not involved in the methylation of Rubisco.

SAFE1 Is a Suppressor of the $^1O_2$-Induced EX1-Independent Pathway. When screening for suppressors of the *flu ex1* mutant, we envisaged three possible scenarios: 1) identification of a negative regulator acting in the $^1O_2$-induced EX1-dependent signaling pathway, 2) identification of a negative regulator that suppresses an unknown downstream component (designated as X) of

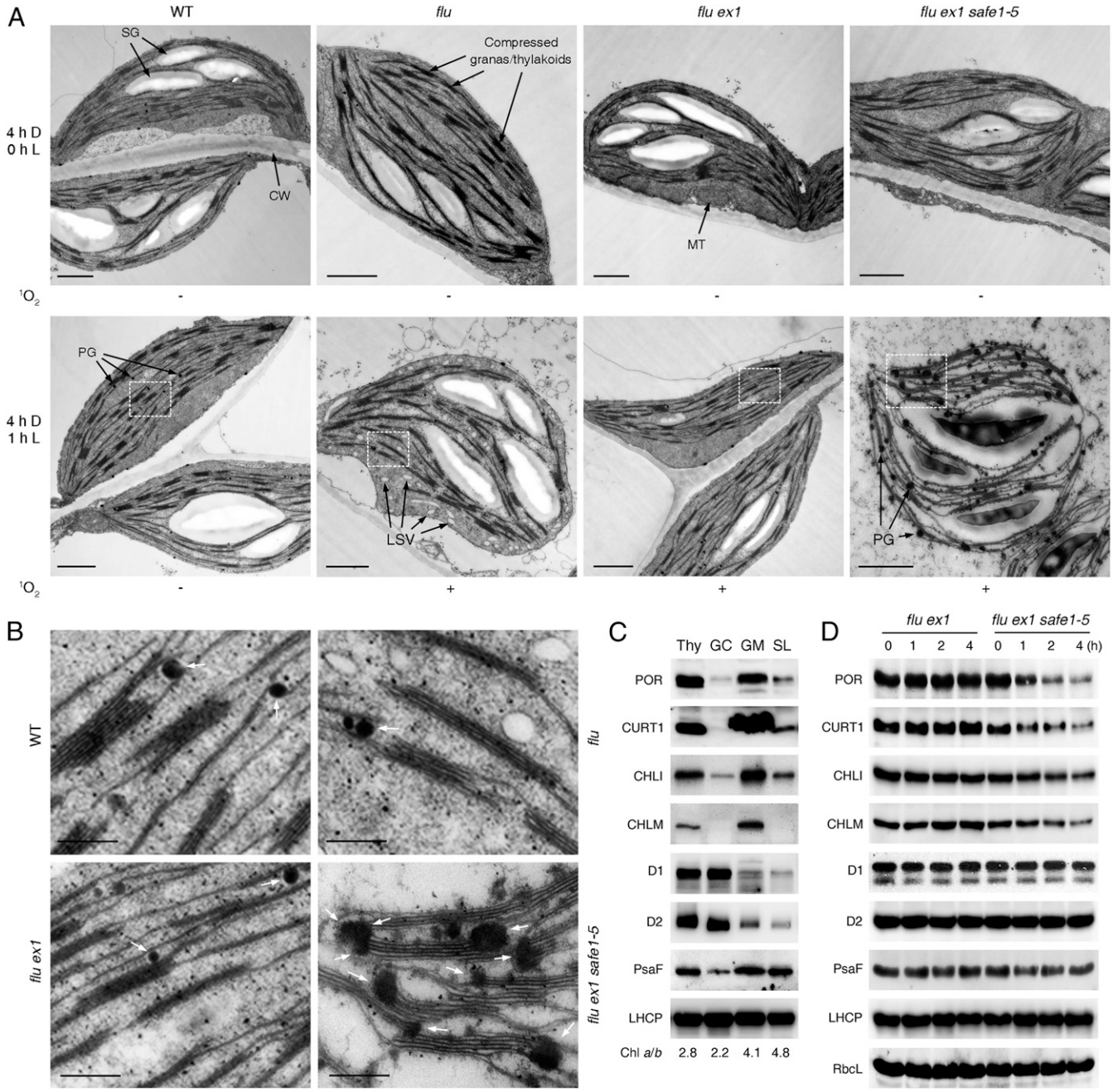

Fig. 3. SAFE1 protects the GMs from $^1O_2$-induced damages. (*A*) Representative electron micrographs of chloroplasts in 6-d-old WT, *flu*, *flu ex1*, and *flu ex1 safe1–5* seedlings before and after release of $^1O_2$. Release of $^1O_2$ in *flu*, *flu ex1*, and *flu ex1 safe1–5* seedlings was achieved by exposing D-incubated (4-h) seedlings to L for 1 h (4-h D, 1-h L). The status of $^1O_2$ generation is shown below the corresponding electron micrographs. Note that chloroplasts from WT and *flu ex1* were intact while those from *flu* and *flu ex1 safe1–5* were damaged. Starch granule (SG); cell wall (CW); mitochondrion (MT); plastoglobule (PG); low staining vesicles (LSV). Bar = 1,000 nm. (*B*) Enlargement of the areas marked by white rectangles in *A* to show accumulation of PGs (indicated by white arrows) on the GMs of *flu ex1 safe1–5*. Bar = 250 nm. (*C*) Confirmation of the subcellular localization of the representative GC-, GM-, and SL-enriched proteins in purified Thy and Thy subfractions (GC, GM, and SL) by Western blot analysis. The chlorophyll *a*/*b* ratio in each fraction is indicated below the Western blot results. (*D*) In *flu ex1 safe1*, release of $^1O_2$ induces degradation of GM-enriched (POR, CURT1, CHLI, and CHLM), but not of GC-enriched (D1 and D2) proteins, as determined by Western analysis (see *Methods*). Total proteins were extracted from 6-d-old *flu ex1* and *flu ex1 safe1–5* seedlings that were kept in the D for 4 h and exposed to L for 0–4 h as indicated.

EX1-dependent $^1O_2$-induced signaling, or 3) identification of a negative component that suppresses an EX1-independent pathway (Fig. 5*A*). In scenario 1, the mutation of SAFE1 would abrogate its inhibitory effect and lead to constant activation of downstream signaling, causing constitutive cell death in plants lacking a functional SAFE1 protein. In scenario 2, lack of the functional SAFE1 protein would also cause constitutive cell death independent of the *flu* mutation. In scenario 3, the negative regulator SAFE1 would "bypass" EX1-dependent signaling, and SAFE1 action would then be dependent on the release of $^1O_2$ (the *flu* mutation). The *safe1* single mutant would not display a cell-death phenotype (because no $^1O_2$

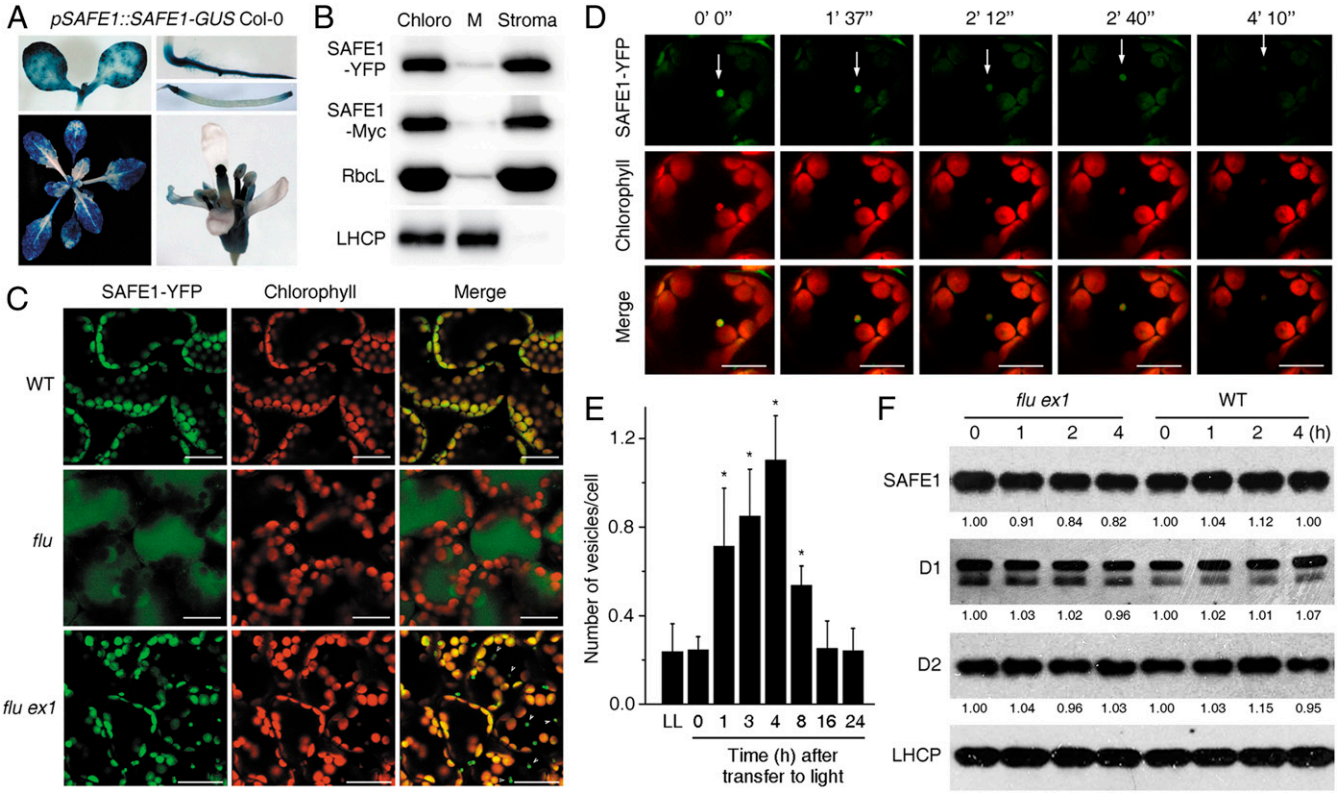

Fig. 4. $^1O_2$ induces degradation of the chloroplast stroma-localized SAFE1 protein. (*A*) Expression analysis of *SAFE1-GUS* at different developmental stages. (*B*) Suborganellar localization of tagged SAFE1 proteins using Western analysis. Marker proteins were RbcL (stroma) and light-harvesting chlorophyll *a*/*b* binding protein (LHCP) (chloroplast membrane = M). Total chloroplasts (Chloro). (*C*) The fate of SAFE1 after release of $^1O_2$. In the WT (*pSAFE1::SAFE1-YFP* Col-0) SAFE1-YFP was evenly distributed in the chloroplasts as no $^1O_2$ was generated. Release of $^1O_2$ caused chloroplast rupture in the *flu* (*pSAFE1::SAFE1-YFP flu*) mutant but induced the formation of SAFE1-containing vesicles originating from chloroplasts in *flu ex1* (*pSAFE1::SAFE1-YFP flu ex1*). Generation of $^1O_2$ was achieved by first keeping 6-d-old seedlings in the D for 4 h and then in the L for an additional 4 h. Bar = 20 μm. (*D*) The degradation process of a representative SAFE1-containing vesicle (indicated by white arrows) in *pSAFE1::SAFE1-YFP flu ex1* seedlings. A series of confocal images was taken from 6-d-old seedlings that were first kept in the D for 4 h and then exposed to L for 4 h. Imaging times are indicated on top of the corresponding images. Bar = 20 μm. (*E*) Statistics of $^1O_2$-induced vesicles in *pSAFE1::SAFE1-YFP flu ex1*. Vesicles were counted from 10 confocal images representing ~200 cells at each time point. Asterisks indicate significant differences ($P < 0.05$, *t* test) compared to the seedlings grown under continuous light (LL). Generation of $^1O_2$ was achieved by keeping 6-d-old seedlings in the D for 4 h and then in the L for 0–24 h as indicated. (*F*) The overall SAFE1 content was not dramatically reduced by $^1O_2$. Total proteins were extracted from 6-d-old seedlings that had been incubated in the D for 4 h and reexposed to L for 0–4 h as indicated, and relative amounts of SAFE1, D1, and D2 were measured. The LHCP protein was used as the loading control.

would be generated in this genetic background), and the *flu safe1* double mutant would show a stronger phenotype than *flu* and *flu ex1 safe1* because two $^1O_2$-induced pathways would be activated in *flu safe1* simultaneously.

To ascertain which (if any) of these models applied, phenotypes of the *safe1* and *flu safe1* mutants were studied in comparison with the known phenotypes of *flu*, *flu ex1*, and *flu ex1 safe1* mutants (Fig. 1). The *safe1* single-mutant seedlings exhibited no $^1O_2$-induced stress responses upon a D–L shift (Fig. 5 *B*–*D*), nor did the *safe1* mutant accumulate Pchlide in the D (Fig. 5*E*), and no $^1O_2$ was generated after a D–L shift (Fig. 5*F*). The *flu safe1* and *flu ex1 safe1* seedlings accumulated similar amounts of Pchlide in the D (Fig. 5*E*) and generated similar amounts of $^1O_2$ after transfer to L (Fig. 5*F*). However, compared with *flu ex1 safe1*, the *flu safe1* double mutant showed much more prominent $^1O_2$-induced stress responses, including bleaching of cotyledons (Fig. 5*B*), decrease in transient chlorophyll fluorescence (Fig. 5*C*), and reduced maximum quantum efficiency of PSII (F_v/F_m) (Fig. 5*D*) after a D–L shift. To confirm these differences in the magnitude of $^1O_2$-induced stress responses in mature plants, all three mutants were exposed to a L/D/dim-L regime (Fig. 5*G*) in which less $^1O_2$ was produced. This is because the rate of $^1O_2$ generation is dependent on both the amount of Pchlide accumulated in the D and the L intensity during reillumination (26). With reduced $^1O_2$ levels, the mature *flu* mutant showed weak, the *flu ex1 safe1* mutant showed stronger, and the *flu safe1* mutant showed the strongest cell-death responses (Fig. 5 *G* and *H*). The levels of $^1O_2$-induced stress responses based on the decrease in F_v/F_m values, Pchlide accumulation, and $^1O_2$ generation in all tested mutant lines are summarized in Fig. 5*I*, and they agree with predictions based on scenario 3 as shown in Fig. 5*A*. Therefore, we postulate that SAFE1 acts as a negative regulator in a $^1O_2$-induced EX1-independent pathway. However, it is still unclear whether the $^1O_2$-EX1 and $^1O_2$-SAFE1 pathways converge on same downstream component(s).

Discussion

Here, we have identified a $^1O_2$-induced and EX1-independent retrograde signaling pathway that is suppressed by SAFE1. In *flu ex1 safe1* plants, $^1O_2$-induced responses return to the same or higher levels than those seen in the *flu* mutant (Fig. 1 and *SI Appendix*, Figs. S1 and S3), while under LL without $^1O_2$ generation, *flu ex1 safe1* plants behave like WT (Fig. 1 and *SI Appendix*, Figs. S1 and S4). However, a slight increase in $^1O_2$ content suffices to initiate a cell-death response in *flu ex1 safe1* (Fig. 1 *C*–*G*), although not in *flu*. Given that similar amounts of

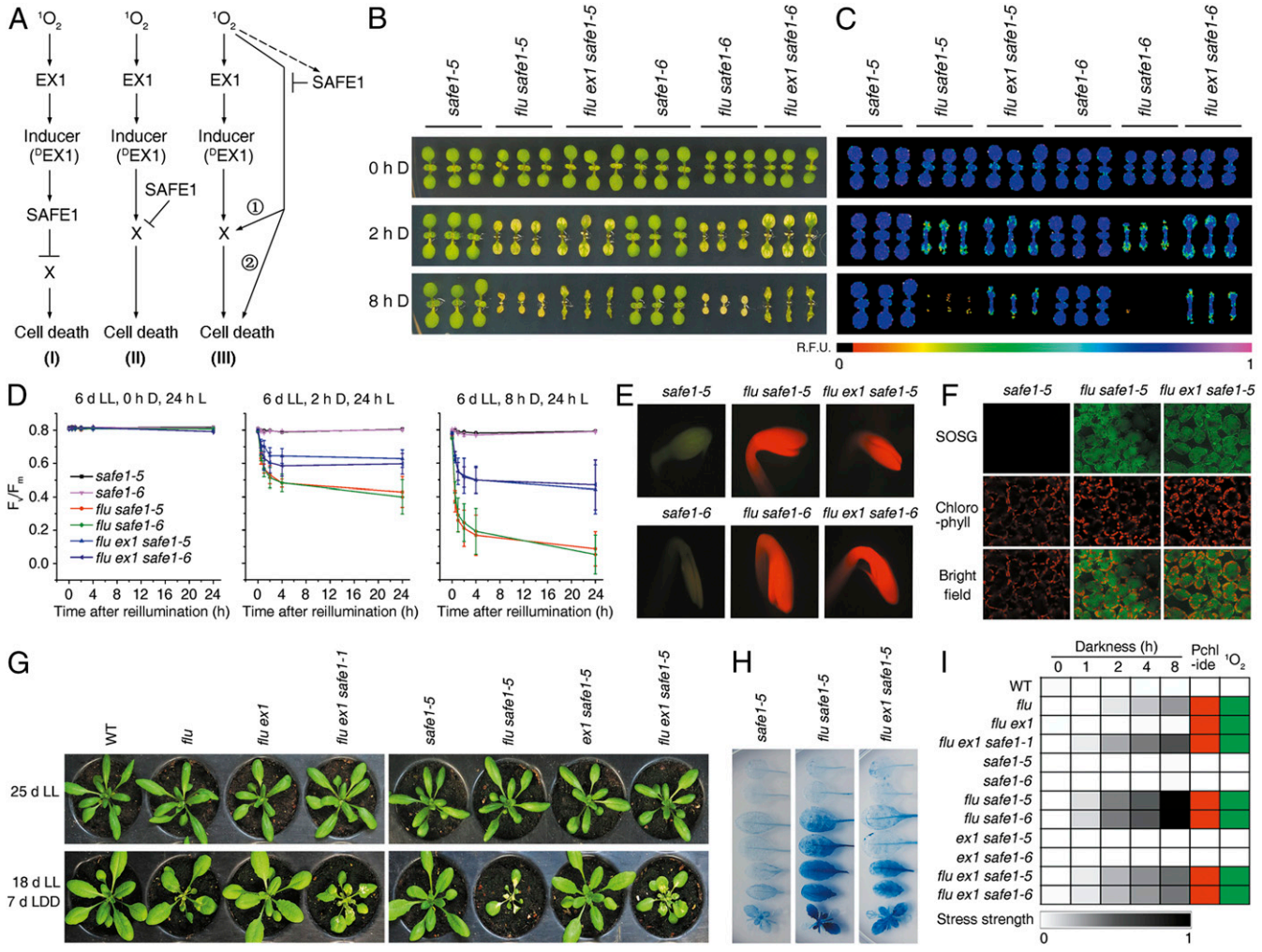

Fig. 5. SAFE1 is a suppressor of $^1O_2$-induced, EX1-independent signaling. (*A*) Possible modes of SAFE1 function. SAFE1 might operate as a negative regulator downstream of EX1 (*I*), negatively regulate an unknown downstream component (*II*), or act in an EX1-independent pathway (*III*). In the latter case, *flu safe1* plants should display a very strong $^1O_2$-induced stress response, whereas *safe1* plants should behave like WT. (*B–D*) $^1O_2$-induced stress responses are enhanced in *flu safe1* and absent in *safe1* as indicated by levels of cotyledon bleaching (*B*), chlorophyll autofluorescence (*C*), and F_v/F_m values (*D*). Different levels of $^1O_2$ generation were achieved by incubating seedlings in the D as indicated. Mean values ± SDs ($n > 30$) are provided. (*E*) Direct visualization of Pchlide accumulation in 4-d-old etiolated seedlings. While *safe1* plants did not accumulate Pchlide, *flu safe1* and *flu ex1 safe1* accumulated similar amounts of Pchlide. (*F*) Detection of $^1O_2$ generation by using SOSG. (*G*) Cell-death response after moderate $^1O_2$ generation. Note that *flu* shows a weak response, while *flu ex1 safe1* and *flu safe1* exhibit stronger and strongest effects, respectively. LDD, light/dark/dim-light. (*H*) $^1O_2$-induced cell death responses in mature leaves of *safe1*, *flu safe1*, and *flu ex1 safe1*. (*I*) A heatmap illustrates and summarizes Pchlide accumulation, $^1O_2$ generation, and corresponding $^1O_2$-induced stress strengths based on the decrease in F_v/F_m in all mutants examined in this study.

$^1O_2$ are generated upon reillumination of D-adapted *flu* and *flu ex1 safe1* seedlings (Fig. 1 *H–J*) and similar sets of genes are induced by it (Fig. 2), the $^1O_2$ released in *flu ex1 safe1* is apparently acting primarily as a signal rather than as a cytotoxin. Moreover, SAFE1 is not a quencher of $^1O_2$ because levels of $^1O_2$ in *flu*, *flu ex1*, *flu safe1*, and *flu ex1 safe1* are comparable to each other (Figs. 1*J* and 5*F*).

Previous studies have shown that chloroplasts are the source and primary target of $^1O_2$-mediated cell-death responses (16) and play an important role in initiating disease and defense signals (34). Our present paper indicates that, in a chloroplast, the GM is the first target of $^1O_2$ and a damaged GM initiates a stress signaling (Fig. 3). Enzymes of tetrapyrrole biosynthesis are highly enriched in the GM (Fig. 3*C*) (17), indicating that Pchlide is first synthesized in the GM. However, when the *flu* or *flu ex1* plants are incubated in the D for a longer time (8 h), Pchlide accumulates significantly not only in the GM, but also in the GC and slightly in the SL and generates $^1O_2$ there after reillumination (17). Compared with the GC, the GM is prone to be damaged by $^1O_2$. In *flu ex1 safe1*, the $^1O_2$-induced damage on the GM is evidenced by the drastic decrease in GM proteins, especially the POR proteins (Fig. 3*D*). In plants, the POR proteins are responsible for the photoreduction of Pchlide to chlorophyllide (Chlide) under L (35) and, thus, might be very close to the site of $^1O_2$ generation when the D-incubated *flu ex1 safe1* plants are transferred to L. This might be why the POR proteins are those that are most severely damaged when $^1O_2$ is released in *flu ex1 safe1* (Fig. 3*D*). The specific and severe degradation of the GM proteins provides direct evidence that the GM is the first target of $^1O_2$. PGs are Thy-associated droplets that function in metabolite biosynthesis, repair, and disposal, and their numbers and sizes increase upon oxidative stress and during senescence (36). Under normal or high-L stress conditions, the PGs randomly associate with Thys (37). However, in *flu ex1 safe1*, enlarged and clustered PGs accumulate on the GM after release of $^1O_2$, providing additional evidence that the GM is the primary target

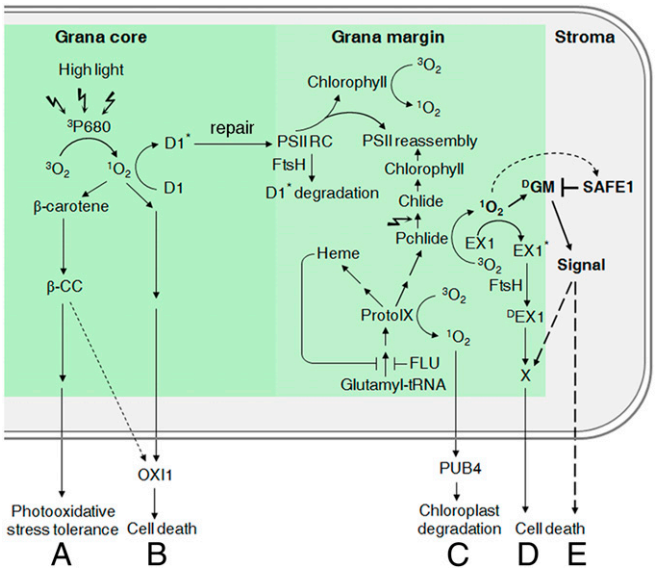

Fig. 6. A model summarizing $^1O_2$-induced signaling pathways in the chloroplast. (*A*) Under high L, $^1O_2$ is mainly produced in the GC (PSII RC) by transfer of energy from excited triplet state P680 chlorophyll (^{3}P680) to ground state oxygen ($^3O_2$) (43). The $^1O_2$ produced in the PSII RC leads to rapid turnover of the D1 protein (43) and oxidizes β-carotene (29). The β-carotene oxidation product β-CC can induce a signaling cascade that confers plant tolerance to photo-oxidative stress (29). (*B*) $^1O_2$ produced in the PSII RC can also lead to programmed cell death (PCD) via a pathway that involves OXI1 kinase and jasmonic acid (JA) (12). (*C*) In the GMs, $^1O_2$ is mainly produced from intermediates of tetrapyrrole biosynthesis (Pchlide, ProtoIX) (11, 17) and in lesser amounts from free chlorophyll resulting from PSII RC turnover (59). $^1O_2$ generated from ProtoIX damages the chloroplasts, which are subsequently ubiquitinated and degraded. This process involves the E3 ubiquitin ligase PUB4 and is independent of the EX1 protein (11). (*D*) However, when $^1O_2$ is produced from Pchlide, EX1 is necessary for initiating another signaling transduction cascade (10). $^1O_2$ generated from Pchlide oxidizes proteins nearby, including EX1. The oxidized EX1 proteins are then cleaved by the FtsH protease, and the proteolysis products of the EX1 protein (^{D}EX1) probably serve as a signal to induce PCD in young seedlings and growth inhibition in mature plants (17, 19). (*E*) The $^1O_2$ generated from Pchlide can induce an EX1-independent signaling pathway that is suppressed by the SAFE1 protein. The stroma-localized SAFE1 protein is a negative regulator and functions as a "protector" of GMs. Without this protector, $^1O_2$ generated from Pchlide would damage GMs, and the damaged GMs (^{D}GM) would initiate EX1-independent signaling and would lead to cell death in young seedlings and growth inhibition of mature plants. The signaling cascades suggested by recent studies are indicated by solid arrows, while the predicted cascades are shown by dashed arrows.

of *flu*-generated $^1O_2$ (Fig. 3) and that SAFE1 protects the GM from $^1O_2$-induced damage. Compared to the GM, the highly compressed GC is physically more robust as evidenced by its resistance to a mild detergent treatment while the same treatment breaks down the GM from Thys (38). The relative robustness might explain why the GC is not apparently damaged by *flu*-generated $^1O_2$. GMs are curved areas of Thys, and the spaces between lipid molecules are bigger than that in the GC. This curved structure might make the GM vulnerable to $^1O_2$ and, in turn, highlights the need of a "safeguard."

In plants, three mechanisms have been distinguished previously to cope with $^1O_2$ stress in the chloroplast: rapid turnover of PSII RC proteins (39, 40), chloroplast rupture (16, 17), and selected degradation of entire chloroplasts (11, 41). Intriguingly, the scenario that occurs in *flu ex1* seedlings after $^1O_2$ stress is different from the three mechanisms and might represent a new strategy. In *flu ex1*, the content of PSII RC proteins D1 and D2 is not significantly affected (Figs. 3*D* and 4*F*), and the chloroplasts are still intact after release of $^1O_2$ (Figs. 3*A* and 4*C*) (17). After release of $^1O_2$, a small fraction of SAFE1 is enriched in distinctive loci of the chloroplast and degraded via formation of chloroplast-originated SAFE1-containing vesicles in *flu ex1* plants (Fig. 4 *C* and *D*). For plants, this might be the most economical way to deal with $^1O_2$ stress. In this way, only a small fraction of chloroplast proteins are expelled and degraded, and the whole chloroplast is still intact and functional. The unapparent degradation of the SAFE1 protein might be explained by the discordance between the localization of SAFE1 and the site of $^1O_2$ production. Since $^1O_2$ is mainly produced at Thys (17) and SAFE1 is localized in the stroma, only a small part of the SAFE1 protein is in direct contact with and can be damaged by $^1O_2$. The $^1O_2$-induced SAFE1-containing vesicles resemble the already described stress-induced chloroplast vesiculation-containing vesicles in their size, content, and formation/degradation process (Fig. 4 *C* and *D* and *SI Appendix*, Fig. S8) (42). However, more experiments are needed to fully understand this strategy that is employed by plants to cope with $^1O_2$ stress.

Several $^1O_2$-induced chloroplast signaling pathways have been reported (10–12, 29) (Fig. 6). In the GC region, $^1O_2$ is mainly produced in the PSII RC under stress conditions (43) where it induces two signaling relays: the 1) β-CC-mediated (29) and 2) OXI1 kinase-mediated (12) pathways. In the GM region, $^1O_2$ is generally produced from tetrapyrrole biosynthesis intermediates, and there, it triggers two other pathways: 1) EX1/EX2-dependent programmed cell death (10, 28) and 2) selective degradation of the entire chloroplast activated by the E3 ubiquitin ligase plant U-box 4 (PUB4) (11). Our results now allow us to define a third GM-associated and $^1O_2$-induced pathway, the $^1O_2$-SAFE1 pathway, which does not require EX1 and is negatively regulated by SAFE1. Activation of this pathway results in cell death of young seedlings and growth inhibition of mature plants (Fig. 1 and *SI Appendix*, Fig. S1), and SAFE1 suppresses this pathway by inhibiting $^1O_2$-induced damages on GMs (Fig. 3 and *SI Appendix*, Fig. S7). While SAFE1 can suppress $^1O_2$-induced signaling originating from the GM, it apparently has limited effects on GC-associated $^1O_2$-induced signaling because 1) under high-L stress, *safe1*, *flu safe1*, and *flu ex1 safe1* seedlings behave like WT (*SI Appendix*, Fig. S5), 2) the *reSAFE1* gene set shows little overlap with high-L-induced genes (Fig. 2*D*), and 3) the soluble SAFE1 protein is localized in the stroma (Fig. 4*B*) and might not have easy access to the GC. A model summarizing the current understanding of $^1O_2$-induced signaling pathways in chloroplasts is shown in Fig. 6.

Methods

Plant Materials and Growth Conditions. All mutants used in this study are in the Col-0 background unless otherwise stated. Seeds were surface sterilized with 0.6% (vol/vol) sodium hypochlorite solution containing 0.01% (vol/vol) Triton X-100 for 10 min and then washed four times with double distilled water. After stratification at 4 °C for 2 d, seeds of WT, *flu*, *flu ex1*, *flu ex1 safe1*, *safe1*, and complemented lines were grown either on soil or on 1/2 MS medium (with 0.5% [m/v] sucrose and 0.8% [m/v] plant agar) for 6 d under LL (100 μmol of photons m^{-2} s^{-1}) or under long-day conditions (LD; 16-h L/8-h D) at 22 °C. These seedlings were further grown under LL or incubated in the D for 0–8 h and transferred to L for various lengths of time (as indicated in the figures) to generate $^1O_2$.

Mutagenesis of *Arabidopsis flu ex1* and Screening of Suppressor Mutants. Mutagenesis of the *A. thaliana flu ex1* mutant was performed using EMS according to Kim et al. (44) Approximately 100,000 M2 seeds from 5,000 M1 plants were sown on soil at a density of 10,000 seeds m^{-2}. After stratification at 4 °C for 2 d, seeds were grown under LL for 14 d and then transferred to LD for 4 d. Plants showing cell-death responses were recognized as candidate suppressor mutants and transferred to LL and grown to maturity.

Identification of the *SAFE1* Gene. To identify the mutated *SAFE1* gene, the *flu ex1 safe1* (Col-0) mutant was crossed with *flu ex1* (Ler). F2 plants were first grown under LL for 14 d and then under LD for 4 d. Approximately 200 from

the 800 plants showing the typical cell-death responses were grown under LL for another 10 d. Leaves from these 200 plants were pooled, ground in liquid nitrogen, and suspended in 100-mL nuclear lysis buffer (0.4-M sucrose, 10-mM Tris·HCl [pH 7.0], 1% [vol/vol] β-mercaptoethanol, 1% [vol/vol] Triton X-100) and kept on ice for 15 min. Then, the suspension was filtered through two layers of Miracloth (Millipore, 475855–1R) into two 50-mL tubes and centrifuged at 3,000 × *g* for 15 min at 4 °C. The resulting pellet was resuspended in 1-mL nuclear lysis buffer, transferred to a 1.5-mL microfuge tube, and centrifuged at 3,000 × *g* for 15 min at 4 °C. The supernatant was discarded, and genomic DNA was extracted from the pellet using the Qiagen DNeasy Plant Mini Kit (Qiagen, 69104). About 2 μg of genomic DNA was subjected to next-generation sequencing. DNA-seq libraries were prepared, and 75-bp paired-end sequencing was conducted on an Illumina NextSeq500 instrument in the Biotechnology Resource Center at Cornell University.

To find the mutation(s) underlying the cell-death response, the sequencing data were processed with the next-generation EMS mutation mapping tool (45). Briefly, the sequencing adapters and low-quality bases were removed from raw reads using Trimmomatic v0.32 (46). The remaining cleaned reads were mapped to the *Arabidopsis* genome TAIR10 (https://www.arabidopsis.org/) using BWA v0.7 (47). The mapped alignment file was sorted and converted to BAM format using SAMtools (48). Next, the duplicated mapped reads were marked using Picard Tools v1.141 (http://broadinstitute.github.io/picard). Then, the single nucleotide polymorphisms were called using SAMtools (48), and the generated Variant Call Format file was converted to the "emap" format file using the BCF2NGM.pl script downloaded from the NGM website. Finally, the preprocessed emap format file was uploaded to NGM (http://bar.utoronto.ca/ngm/cgi-bin/emap.cgi) to identify the mutations associated with the phenotypes.

For the traditional map-based cloning, another 200 plants exhibiting the mutant phenotype were screened, and genomic DNAs were extracted individually. The genotypes of these plants were tested using simple sequence length polymorphism markers found on the *Arabidopsis* mapping platform (https://www.arabidopsis.org/portals/mutants/mapping.jsp).

Complementation of the *flu ex1 safe1* Mutant. For complementation of *flu ex1 safe1*, the genomic region encompassing *SAFE1* (*At5g14260*) was amplified by PCR using the sense primer GCCTCTAAACATTTACCATAGTTTCTG and the antisense primer TTTCAAGGAAGGAGCATATGGTGC. The PCR product was inserted into the entry vector pCR8/GW/TOPO (Invitrogen) and, subsequently, cloned to the destination vectors pGWB516 (which adds a C-terminal 4×Myc tag), pGWB533 (which adds a C-terminal GUS tag), and pGWB540 (which adds a C-terminal EYFP tag) (49) via the Gateway LR cloning reaction (Invitrogen). All these constructs were transformed into *Agrobacterium tumefaciens* strain GV3101 and transferred to *flu ex1 safe1* plants by floral dipping (50).

Isolation and Fractionation of Chloroplasts. Chloroplasts were isolated and fractionated into membrane and stroma fractions as described by Kauss et al. (15) Fractionation of the Thy membrane into the GC, GM, and SL was performed as described by Wang et al. (17)

Measurement of F_v/F_m, PSII Operating Efficiency, Nonphotochemical Quenching, and Pulse-Amplitude Modulated Traces. The maximum quantum efficiency of PSII (F_v/F_m), PSII operating efficiency (ΦPSII), nonphotochemical quenching, and pulse-amplitude modulated (PAM) traces (51) were recorded using an automatic PAM fluorometer (Imaging PAM, Walz) following the manual provided by the manufacturer.

Trypan Blue Staining of Dead Cells. Trypan blue staining of dead cells was performed as described by op den Camp et al. (9).

Extraction and Determination of Pchlide and Chlide. Pchlide and Chlide were extracted and measured as described by Yoshida et al. (52). Tetrapyrroles were extracted from D-treated WT, *flu*, *flu ex1*, and *flu ex1 safe1* seedlings or mature leaves with a buffer containing 80% (vol/vol) acetone and 0.0083% (vol/vol) ammonia overnight at 4 °C in the D. An equal volume of 80% acetone-saturated hexane was added, and the solution was mixed well by vortexing. After centrifugation at 5,000 × *g* for 10 min at 4 °C, the acetone phase (lower layer) was transferred to a new tube and washed again with an equal volume of 80% (vol/vol) acetone-saturated hexane. The resulting acetone solution, thus obtained, contained no detectable chlorophyll. Fluorescence emission spectra (600–720 nm) excited at a wavelength of 433 nm were recorded at room temperature (RT) using a LS50 luminescence spectrophotometer (Perkin-Elmer). Acetone (80%) was used as a reference. Pchlide has its absorption peak at 634 nm and Chlide at 673 nm.

Direct Visualization of Pchlide Accumulation in Etiolated Seedlings. To obtain etiolated seedlings, surface-sterilized seeds of WT, *flu*, *flu ex1*, *flu ex1 safe1*, *safe1*, and/or *flu safe1* were sown on 1/2 Murashige and Skoog medium and grown in the D at 22 °C for 4 d. For direct visualization of Pchlide accumulation, etiolated seedlings were illuminated with blue L and examined using a fluorescence microscope (Olympus SZX-12). The bright red fluorescence emitted by the mutants lacking a functional FLU protein is caused by excitation of Pchlide.

GUS Staining. GUS staining was performed according to Wang et al. (53).

Confocal Imaging. Confocal imaging was performed with a Leica TCS SP5 laser scanning confocal microscope. EYFP was excited with the 514-nm line of an argon laser, and the emission was recorded by passing through the filter bandpass (BP) 535/30 and false-colored green. GFP was excited with the 488-nm line of an argon laser, and the emission from 510 to 544 nm was recorded with the BP 525/50 filter and colored green. Chlorophyll autofluorescence was excited with the 458-nm line of the argon laser, and the emission was recorded in the range of 650–700 nm.

Measurement of the Production of $^1O_2$. $^1O_2$ was quantified using SOSG (Invitrogen, S36002) as described by Flors et al. (54). WT, *flu*, *flu ex1*, and *flu ex1 safe1* seeds were grown on soil under LL for 6 d and incubated in the D for 4 h. Hypocotyls were immersed in a solution containing 260-μM SOSG and 50-mM sodium phosphate buffer (pH 7.5). The shoots were allowed to transpire for another 3 h in the D and transferred to L for 40 min. The $^1O_2$-activated SOSG signal was recorded using a Leica TCS SP5 laser scanning confocal microscope with excitation at 488 nm, and the emission from 510 to 600 nm was collected.

RNA-seq, Data Analysis, and Quantitative RT-PCR. Total RNAs from *Arabidopsis* seedlings were isolated using TRIzol (Invitrogen) and purified using Direct-zol RNA MiniPrep Plus columns (Zymo Research) according to the manufacturer's instructions. RNA integrity and quality were assessed with an Agilent 2100 Bioanalyzer. Ribosomal RNA depletion, generation of RNA-seq libraries, and 150-bp paired-end sequencing on an Illumina HiSeq 2500 system were conducted at Novogene Biotech (Beijing, China) with standard Illumina protocols. Two independent biological replicates were used per genotype.

RNA-seq reads were analyzed on the Galaxy platform (https://usegalaxy.org/). After grooming FASTQ files, adaptors were removed with Trimmomatic (46), and sequencing quality was accessed with FastQC (http://www.bioinformatics.babraham.ac.uk/projects/fastqc/). Reads were mapped to the *Arabidopsis* genome (TAIR10) with the gapped-read mapper TopHat 2.1.1 (55) set for Forward Read unstranded libraries and adjusting the maximum intron length to 5,000 bp. Reads were counted with featureCounts (56) with the help of the gene annotation in Araport11 (https://www.arabidopsis.org/download/index-auto.jsp?dir=%2Fdownload_files%2FGenes%2FAraport11_genome_release). Differentially expressed genes were obtained with DESeq2 (57) applying a twofold change cutoff and an adjusted $P < 0.05$. Sequencing data have been deposited in NCBI's Gene Expression Omnibus (GEO) database, https://www.ncbi.nlm.nih.gov/geo (58) (accession no. GSE131610).

For quantitative RT-PCR, cDNA was synthesized from 1 μg of total RNA using the iScript cDNA synthesis kit (Bio-RAD, Cat. no. 1708890) following the instructions provided with the kit. Quantitative RT-PCR was performed with an iQ5 multicolor real-time detection system (Bio-RAD). Expression of the detected genes was normalized to *Actin2*, and primers used in this study are listed in Dataset S7.

Protein Extraction and Western Blot Analysis. Shoots (about 100 mg) of 6-d-old seedlings were frozen in liquid nitrogen and ground to a fine power. Proteins were extracted by adding 1 mL of protein extraction buffer (20-mM Hepes [pH 7.4], 2-mM [ethylenedinitrilo]tetraacetic acid [pH 7.4], 2-mM ethylene glycol bis[β-aminoethyl ether]-*N*,*N*,*N*′,*N*′-tetraacetic acid [pH 7.4], 25-mM NaF, 1-mM Na_3VO_4, 50-mM glycerophosphate, 100-mM NaCl, 0.5% [vol/vol] Triton X-100, 10% [vol/vol] glycerol, 1× SIGMAFAST Protease Inhibitor) and incubated on ice for 30 min. After centrifugation at 12,000 × *g* for 30 min at 4 °C, the clear supernatant was transferred to 15-mL Falcon conical centrifuge tubes. After addition of 9 mL of 100% acetone, 50 μL of 0.5-M Na_2CO_3, and 50 μL of 0.5-M DTT, the supernatant was mixed well and incubated at −20 °C for 30 min. Proteins were pelleted by centrifugation at 3,000 × *g* for 3 min. The pellet was dried for 10 min at RT and dissolved in 200 μL of 1× Laemmli buffer by heating at 75 °C for 20 min with agitation (500 rpm).

Proteins were normalized to the content of chlorophyll and then fractionated on 10% or 12% sodium dodecyl sulfate-polyacrylamide gel electrophoresis gels, depending on the calculated molecular weight of the target protein and were then transferred to a polyvinylidene difluoride membrane (Millipore, IPVH00010). The membrane was blocked for 1 h with 5% skim milk in 1× TBS (50-mM Tris·HCl [pH 7.5] and 150- mM NaCl) and incubated overnight at 4 °C using antiserum against GFP (Sigma-Aldrich, G1546), Myc (Santa Cruz Biotechnology, sc-40), RbcL (Agrisera, AS03 037), LHCP (AS01 004), D1 (AS11 1786), D2 (AS06 146), PsaF (PSI subunit F; AS06 104), POR (AS05 067), CURT1A, CHLI, or CHLM. The antibody solution was decanted, and the blot was washed for 4 × 10 min with 1× TBST (50-mM Tris·HCl [pH 7.5], 150-mM NaCl, 0.1% Tween-20) at RT. Then the blot was incubated with either anti-rabbit IgG-HRP (Santa Cruz Biotechnology, sc-2004) or anti-mouse IgG-HRP (Santa Cruz Biotechnology, sc-2005) at RT for 1 h with slow agitation. The blot was washed for 4 × 10 min with 1× TBST and developed with an enhanced chemiluminescence substrate (Thermo Scientific, 32106). Fluorescence was recorded using a CCD camera (Peqlab, Fusion Fx7).

ACKNOWLEDGMENTS. We thank T. Nakagawa for providing *pGWB516*, *pGWB533*, and *pGWB540* vectors; B. Grimm and B. Hedtke for antisera (CHLI and CHLM); V. Dogra and C. Kim for RNA-seq data of *flu*; M. Srivastava, S. Schwenkert, and H. Harz for helping with confocal imaging; Z. Fei and A. Klingl for help with DNA-seq data analysis and transmission electron spectroscopy, respectively; and C. Kim and X. Xu for help in the initial phase of this work. This work was supported by National Institutes of Health Grant R01-GM085036 (to K.A.), and Grants from the Deutsche Forschungsgemeinschaft to D.L. and T.K. (KL 2362/1-1 and TRR175, Projects C01 and C05).

1. K. Apel, H. Hirt, Reactive oxygen species: Metabolism, oxidative stress, and signal transduction. *Annu. Rev. Plant Biol.* **55**, 373–399 (2004).
2. C. H. Foyer, G. Noctor, Redox regulation in photosynthetic organisms: Signaling, acclimation, and practical implications. *Antioxid. Redox Signal.* **11**, 861–905 (2009).
3. G. Noctor, J. P. Reichheld, C. H. Foyer, ROS-related redox regulation and signaling in plants. *Semin. Cell Dev. Biol.* **80**, 3–12 (2018).
4. R. Mittler, ROS are good. *Trends Plant Sci.* **22**, 11–19 (2017).
5. X. J. Xia *et al*., Interplay between reactive oxygen species and hormones in the control of plant development and stress tolerance. *J. Exp. Bot.* **66**, 2839–2856 (2015).
6. R. Schmidt, J. H. M. Schippers, ROS-mediated redox signaling during cell differentiation in plants. *Biochim. Biophys. Acta* **1850**, 1497–1508 (2015).
7. S. Gilroy *et al*., ROS, calcium, and electric signals: Key mediators of rapid systemic signaling in plants. *Plant Physiol.* **171**, 1606–1615 (2016).
8. C. Triantaphylidès *et al*., Singlet oxygen is the major reactive oxygen species involved in photooxidative damage to plants. *Plant Physiol.* **148**, 960–968 (2008).
9. R. G. L. op den Camp, Rapid induction of distinct stress responses after the release of singlet oxygen in Arabidopsis. *Plant Cell* **15**, 2320–2332 (2003).
10. D. Wagner *et al*., The genetic basis of singlet oxygen-induced stress responses of *Arabidopsis thaliana*. *Science* **306**, 1183–1185 (2004).
11. J. D. Woodson *et al*., Ubiquitin facilitates a quality-control pathway that removes damaged chloroplasts. *Science* **350**, 450–454 (2015).
12. L. Shumbe *et al*., Singlet oxygen-induced cell death in *Arabidopsis* under high-light stress is controlled by OXI1 Kinase. *Plant Physiol.* **170**, 1757–1771 (2016).
13. U. Leisinger *et al*., The glutathione peroxidase homologous gene from Chlamydomonas reinhardtii is transcriptionally up-regulated by singlet oxygen. *Plant Mol. Biol.* **46**, 395–408 (2001).
14. R. Meskauskiene *et al*., FLU: A negative regulator of chlorophyll biosynthesis in *Arabidopsis thaliana*. *Proc. Natl. Acad. Sci. U.S.A.* **98**, 12826–12831 (2001).
15. D. Kauss, S. Bischof, S. Steiner, K. Apel, R. Meskauskiene, FLU, a negative feedback regulator of tetrapyrrole biosynthesis, is physically linked to the final steps of the $Mg^{(++)}$-branch of this pathway. *FEBS Lett.* **586**, 211–216 (2012).
16. C. Kim *et al*., Chloroplasts of *Arabidopsis* are the source and a primary target of a plant-specific programmed cell death signaling pathway. *Plant Cell* **24**, 3026–3039 (2012).
17. L. Wang *et al*., Singlet oxygen- and EXECUTER1-mediated signaling is initiated in grana margins and depends on the protease FtsH2. *Proc. Natl. Acad. Sci. U.S.A.* **113**, E3792–E3800 (2016).
18. V. Dogra *et al*., FtsH2-dependent proteolysis of EXECUTER1 is essential in mediating singlet oxygen-triggered retrograde signaling in *Arabidopsis thaliana*. *Front. Plant Sci.* **8**, 1145 (2017).
19. V. Dogra, M. Li, S. Singh, M. Li, C. Kim, Oxidative post-translational modification of EXECUTER1 is required for singlet oxygen sensing in plastids. *Nat. Commun.* **10**, 2834 (2019).
20. R. Lv *et al*., Uncoupled expression of nuclear and plastid photosynthesis-associated genes contributes to cell death in a lesion mimic mutant. *Plant Cell* **31**, 210–230 (2019).
21. M. Scharfenberg *et al*., Functional characterization of the two ferrochelatases in *Arabidopsis thaliana*. *Plant Cell Environ.* **38**, 280–298 (2015).
22. Q. Ling, P. Jarvis, Plant signaling: Ubiquitin pulls the trigger on chloroplast degradation. *Curr. Biol.* **26**, R38–R40 (2016).
23. F. Ramel *et al*., Light-induced acclimation of the *Arabidopsis chlorina1* mutant to singlet oxygen. *Plant Cell* **25**, 1445–1462 (2013).
24. A. Pruzinská *et al*., In vivo participation of red chlorophyll catabolite reductase in chlorophyll breakdown. *Plant Cell* **19**, 369–387 (2007).
25. J. M. Mach, A. R. Castillo, R. Hoogstraten, J. T. Greenberg, The *Arabidopsis*-accelerated cell death gene *ACD2* encodes red chlorophyll catabolite reductase and suppresses the spread of disease symptoms. *Proc. Natl. Acad. Sci. U.S.A.* **98**, 771–776 (2001).
26. L. Wang, K. Apel, Dose-dependent effects of $^1O_2$ in chloroplasts are determined by its timing and localization of production. *J. Exp. Bot.* **70**, 29–40 (2019).
27. D. Przybyla *et al*., Enzymatic, but not non-enzymatic, $^1O_2$-mediated peroxidation of polyunsaturated fatty acids forms part of the EXECUTER1-dependent stress response program in the *flu* mutant of *Arabidopsis thaliana*. *Plant J.* **54**, 236–248 (2008).
28. K. P. Lee, C. Kim, F. Landgraf, K. Apel, EXECUTER1- and EXECUTER2-dependent transfer of stress-related signals from the plastid to the nucleus of *Arabidopsis thaliana*. *Proc. Natl. Acad. Sci. U.S.A.* **104**, 10270–10275 (2007).
29. F. Ramel *et al*., Carotenoid oxidation products are stress signals that mediate gene responses to singlet oxygen in plants. *Proc. Natl. Acad. Sci. U.S.A.* **109**, 5535–5540 (2012).
30. D. Schnaubelt *et al*., Low glutathione regulates gene expression and the redox potentials of the nucleus and cytosol in *Arabidopsis thaliana*. *Plant Cell Environ.* **38**, 266–279 (2015).
31. H. Cheng, Q. Zhang, D. Guo, Genes that respond to H_2O_2 are also evoked under light in Arabidopsis. *Mol. Plant* **6**, 226–228 (2013).
32. M. Mininno *et al*., Characterization of chloroplastic fructose 1,6-bisphosphate aldolases as lysine-methylated proteins in plants. *J. Biol. Chem.* **287**, 21034–21044 (2012).
33. C. Alban *et al*., Uncovering the protein lysine and arginine methylation network in *Arabidopsis* chloroplasts. *PLoS One* **9**, e95512 (2014).
34. M. de Torres Zabala *et al*., Chloroplasts play a central role in plant defence and are targeted by pathogen effectors. *Nat. Plants* **1**, 15074 (2015).
35. S. I. Beale, Enzymes of chlorophyll biosynthesis. *Photosynth. Res.* **60**, 43–73 (1999).
36. J. R. Austin, 2nd, E. Frost, P. A. Vidi, F. Kessler, L. A. Staehelin, Plastoglobules are lipoprotein subcompartments of the chloroplast that are permanently coupled to thylakoid membranes and contain biosynthetic enzymes. *Plant Cell* **18**, 1693–1703 (2006).
37. C. Bréhélin, F. Kessler, K. J. van Wijk, Plastoglobules: Versatile lipoprotein particles in plastids. *Trends Plant Sci.* **12**, 260–266 (2007).
38. S. Puthiyaveetil *et al*., Compartmentalization of the protein repair machinery in photosynthetic membranes. *Proc. Natl. Acad. Sci. U.S.A.* **111**, 15839–15844 (2014).
39. E. M. Aro, I. Virgin, B. Andersson, Photoinhibition of Photosystem II. Inactivation, protein damage and turnover. *Biochim. Biophys. Acta* **1143**, 113–134 (1993).
40. S. Ohira, N. Morita, H. J. Suh, J. Jung, Y. Yamamoto, Quality control of photosystem II under light stress–turnover of aggregates of the D1 protein *in vivo*. *Photosynth. Res.* **84**, 29–33 (2005).
41. M. Izumi, H. Ishida, S. Nakamura, J. Hidema, Entire photodamaged chloroplasts are transported to the central vacuole by autophagy. *Plant Cell* **29**, 377–394 (2017).
42. S. Wang, E. Blumwald, Stress-induced chloroplast degradation in *Arabidopsis* is regulated via a process independent of autophagy and senescence-associated vacuoles. *Plant Cell* **26**, 4875–4888 (2014).
43. A. Krieger-Liszkay, C. Fufezan, A. Trebst, Singlet oxygen production in photosystem II and related protection mechanism. *Photosynth. Res.* **98**, 551–564 (2008).
44. Y. Kim, K. S. Schumaker, J. K. Zhu, EMS mutagenesis of *Arabidopsis*. *Methods Mol. Biol.* **323**, 101–103 (2006).
45. R. S. Austin *et al*., Next-generation mapping of *Arabidopsis* genes. *Plant J.* **67**, 715–725 (2011).
46. A. M. Bolger, M. Lohse, B. Usadel, Trimmomatic: A flexible trimmer for Illumina sequence data. *Bioinformatics* **30**, 2114–2120 (2014).
47. H. Li, R. Durbin, Fast and accurate short read alignment with Burrows-Wheeler transform. *Bioinformatics* **25**, 1754–1760 (2009).
48. H. Li *et al*.; 1000 Genome Project Data Processing Subgroup, The sequence alignment/map format and SAMtools. *Bioinformatics* **25**, 2078–2079 (2009).
49. T. Nakagawa *et al*., Improved Gateway binary vectors: High-performance vectors for creation of fusion constructs in transgenic analysis of plants. *Biosci. Biotechnol. Biochem.* **71**, 2095–2100 (2007).
50. S. J. Clough, A. F. Bent, Floral dip: A simplified method for *Agrobacterium*-mediated transformation of *Arabidopsis thaliana*. *Plant J.* **16**, 735–743 (1998).
51. T. Rühle, B. Reiter, D. Leister, Chlorophyll fluorescence video imaging: A versatile tool for identifying factors related to photosynthesis. *Front. Plant Sci.* **9**, 55 (2018).
52. K. Yoshida *et al*., Correlated changes in the activity, amount of protein, and abundance of transcript of NADPH:protochlorophyllide oxidoreductase and chlorophyll accumulation during greening of cucumber cotyledons. *Plant Physiol.* **109**, 231–238 (1995).
53. L. Wang *et al*., The *Arabidopsis* purple acid phosphatase AtPAP10 is predominantly associated with the root surface and plays an important role in plant tolerance to phosphate limitation. *Plant Physiol.* **157**, 1283–1299 (2011).
54. C. Flors *et al*., Imaging the production of singlet oxygen *in vivo* using a new fluorescent sensor, Singlet Oxygen Sensor Green. *J. Exp. Bot.* **57**, 1725–1734 (2006).
55. D. Kim *et al*., TopHat2: Accurate alignment of transcriptomes in the presence of insertions, deletions and gene fusions. *Genome Biol.* **14**, R36 (2013).
56. Y. Liao, G. K. Smyth, W. Shi, featureCounts: An efficient general purpose program for assigning sequence reads to genomic features. *Bioinformatics* **30**, 923–930 (2014).
57. M. I. Love, W. Huber, S. Anders, Moderated estimation of fold change and dispersion for RNA-seq data with DESeq2. *Genome Biol.* **15**, 550 (2014).
58. R. Edgar, M. Domrachev, A. E. Lash, Gene expression omnibus: NCBI gene expression and hybridization array data repository. *Nucleic Acids Res.* **30**, 207–210 (2002).
59. B. B. Fischer, É. Hideg, A. Krieger-Liszkay, Production, detection, and signaling of singlet oxygen in photosynthetic organisms. *Antioxid. Redox Signal.* **18**, 2145–2162 (2013).